Available online at www.sciencedirect.com
SCIENCE DIRECT®
ELSEVIER
Mechanical Systems and Signal Processing 20 (2006) 158–187
Mechanical Systems and Signal Processing
www.elsevier.com/locate/jnlabr/ymssp

Monitoring gear vibrations through motor current signature analysis and wavelet transform

Chinmaya Kar, A.R. Mohanty*

Mechanical Engineering Department, Indian Institute of Technology, Kharagpur 721 302, India

Received 15 January 2004; received in revised form 20 July 2004; accepted 25 July 2004
Available online 22 September 2004

Abstract

In gearboxes, load fluctuations on the gearbox and gear defects are two major sources of vibration. Further, at times, measurement of vibration in the gearbox is not easy because of the inaccessibility in mounting the vibration transducers. An efficient and new but non-intrusive method to detect the fluctuation in gear load may be the motor current signature analysis (MCSA). In this paper, a multi-stage transmission gearbox (with and without defects) has been studied in order to replace the conventional vibration monitoring by MCSA. It has been observed through FFT analysis that low frequencies of the vibration signatures have sidebands across line frequency of the motor current whereas high frequencies of vibration signature are difficult to be detected. Hence, discrete wavelet transform (DWT) is suggested to decompose the current signal, and FFT analysis is carried out with the decomposed current signal to trace the sidebands of the high frequencies of vibration. The advantage of DWT technique to study the transients in MCSA has also been cited. The inability of CWT in detecting either defects or load fluctuation has been shown. The results indicate that MCSA along with DWT can be a good replacement for conventional vibration monitoring.

Keywords: Motor current signature; Vibration signature; Discrete wavelet transform; Continuous wavelet transform; Gear load fluctuation; Multi-stage gearbox

*Corresponding author. Tel.: +91-3222-282944; fax: +91-3222-255303.
E-mail address: amohanty@mech.iitkgp.ernet.in (A.R. Mohanty).

0888-3270/$ - see front matter © 2004 Elsevier Ltd. All rights reserved.
doi:10.1016/j.ymssp.2004.07.006

Nomenclature

T	torque in the gearbox
T_0	average torque
ϕ_1, ϕ_2 and ϕ_3	respective phases of f_1, f_2, and f_3
I_{sT}	torque producing component of current
I_{sM}	magnetising current component
I_{sM0} and I_{sT0}	average value of I_{sM} and I_{sT}
I_{sr}	R-phase current component
I_{sy}	Y-phase current component
I_{sb}	B-phase current component
f_e	line frequency in Hz
f_{ecc}	sidebands across f_e due to rotor eccentricity of the induction motor
m	positive integer
s	percentage slip factor of the induction motor
p	no. of poles the induction motor
f_{brb}	sidebands across f_e due to broken rotor bar of induction motor
f_v	characteristics frequencies of bearings
N_s	synchronous speed of the induction motor
N	speed of the induction motor
f_3	output shaft speed of the gearbox
f_3^2	output shaft speed of the gearbox during 2nd gear operation
f_3^3	output shaft speed of the gearbox during 3rd gear operation
f_3^4	output shaft speed of the gearbox during 4th gear operation
f_2	lay shaft speed of the gearbox
f_1	input shaft speed of the gearbox
f_{m2}	tooth-meshing frequency of the 2nd gear pair of the gearbox
f_{m3}	tooth-meshing frequency of the 3rd gear pair of the gearbox
f_{m4}	tooth-meshing frequency of the 4th gear pair of the gear box
$F_J(t)/s$	vibration signal
$\psi(t)$	wavelet function
$\phi(t)$	scale function
γ	coefficient of wavelet function
λ	coefficient of scale function
J, J_0	level of decomposition
$A(i)$	ith level approximation coefficients
$D(i)$	ith level detail coefficients
a	dilation or scale factor
b	data translation or time shifting factor
CWT	CWT coefficients
T_i	the number of teeth in ith gear of the main shaft
T_i^l	the number of teeth in ith gear of the lay shaft

1. Introduction

Gearbox is an important machinery component in any industry. Any defect in gears lead to machine downtime resulting in a loss of production. A number of techniques have been applied in order to diagnose faults in gears. Fast Fourier transform (FFT) is a versatile technique using which the frequency contents of a signal can be found out. Randal and Hee [1] have cited the efficiency of cepstrum analysis in detecting the small sidebands of the tooth mesh frequency. Bayder and Ball [2] have compared acoustic signature with vibration signature using pseudo-Wigner–Ville distribution (WVD), whereas Stander et al. [3] used the pseudo-WVD for detecting faults with fluctuating load condition. Some statistical techniques such as Kolmogorov–Smirnov test [4,5] and autoregressive model [6] have also been tested. Randal [7] has cited an overview of different signal processing techniques related to detection of vibration in turbo-machinery. The most recent and powerful technique that has wide applicability is wavelet transform [6,8–12]. A number of articles have already been published citing advantages of WT over other time–frequency techniques such as WVD and STFT [12–14].

The choice of mother wavelet varies considerably in these literatures. Morlet wavelet has been recommended in continuous wavelet transform (CWT) [6,13] because of its simplicity and similarity with periodic impulses. Gabor-based wavelet was used in [9,11] as it takes smaller area of the frequency window than any other wavelet. Wang and McFadden [8] have suggested using Gaussian-enveloped oscillating wavelet so that the mother wavelet will have similar shape as the small duration transients. But since all the above-mentioned wavelets are non-orthogonal wavelet, these are not appropriate option in dyadic discrete wavelet transform [DWT]. Hence, Sung et al. [10] and Gaborson [13] have used Daubechies 20 and Daubechies 4, respectively, as the mother wavelet. A review of the wavelet application in fault diagnosis has been carried out by Peng and Chu [12].

Application of motor current signature analysis (MCSA) has been limited to monitoring of induction motor and its bearings. Initially, starting current transients were monitored to study torsional vibration [15,16] which was later applied to detect motor bearing damage by Eren and Devany [17] using wavelet analysis. In their paper, the difference in normalized current RMS values of both healthy and faulty bearing has been the basis of fault detection. Schoen and Habetler [18] observing steady currents inferred that the broken rotor, and the eccentricity in rotor and stator of an induction motor result in sidebands of electric supply line frequency. The sidebands are functions of the slip in the induction drive. They also concluded that prior knowledge of the spatial position of fault and load torque with respect to the rotor is necessary as the effects of load torque and faulty conditions are difficult to separate. The work has been extended to online monitoring of induction motor [19,20]. Yacamini et al. [21] inferred that each component of load torque has sidebands across the supply line frequency and they had also applied wavelet transform. MCSA has already been applied to bearing fault diagnosis in Refs. [17,22]. Aller et al. [23] have applied analytic wavelet transform for sensorless speed measurement of AC machines.

The objective of this article is to establish motor current signature analysis as the basis of condition monitoring of a multi-stage gearbox by using DWT. The condition monitoring includes two major sources of vibration: load fluctuation and defects in gears. The following steps are taken to prove the contention of the objective.

1. FFT analysis is used to correlate the components of steady vibration and current signatures. The demerit of this technique lies in the fact that good time resolution will give rise to poor frequency resolution and vice versa, as per the uncertainty principle [14]. Hence, two different sets of data have been acquired to analyse the low-frequency components and the high frequency-components of vibration and current signatures.
2. To eliminate the effect of noise and high-amplitude supply line frequency, FFT analysis is applied to the decomposed steady current signals. These signals are decomposed using DWT with Daubechies 8 (Db8) as the mother wavelet. This choice of the mother wavelet has been chosen for two reasons. First, an orthogonal wavelet for multi-resolution wavelet transform or DWT is required and secondly, the scaling function of 'Db8' shown in Fig. 1(a) matches the transients in motor current.
3. Since, FFT analysis is not suitable for analysing transients, DWT contour plots of the current transients are drawn to distinguish several load fluctuation and defects. CWT is also applied to compare with DWT.

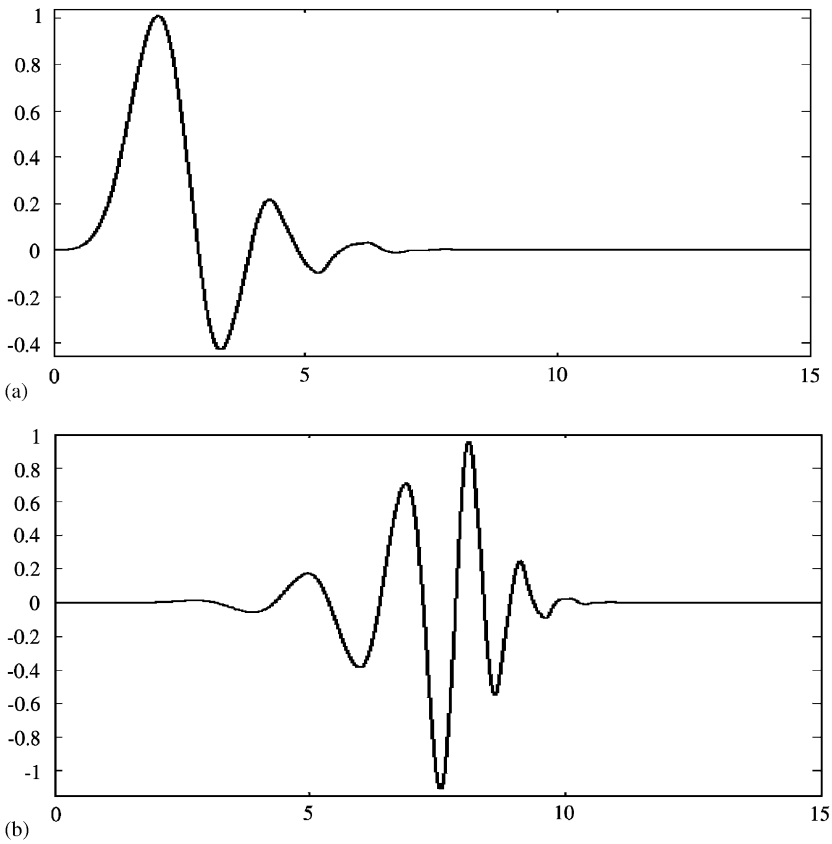

Fig. 1. (a) Scale function, and (b) wavelet function of mother wavelet 'Daubechies 8' ('db8').

2. Theory

2.1. Motor current signature analysis (MCSA)

Whenever there is a load fluctuation, a change in speed occurs thus changing the per unit slip, which subsequently causes changes in sidebands across the line frequency (f_e). But the faults introduced in the components cause magnetic field anomaly thus changing the mutual and self-inductance of motor causing sidebands across line frequency [18]. For different conditions such as eccentricity in rotor (f_{ecc}) and broken rotor bar (f_{brb}), the sidebands of current spectrum are given by following equations:

$$f_{\text{ecc}} = f_e\left[1 \pm m\left(\frac{1-s}{p/2}\right)\right] \tag{1}$$

and

$$f_{\text{brb}} = f_e\left[k\left(\frac{1-s}{p/2}\right) \pm s\right]. \tag{2}$$

In Ref. [22], the characteristics frequencies of vibration signatures of ball bearing (f_v) are shown to have sidebands across the line frequency in the motor current. This is due to the fact that any damage in bearing will cause a change in air gap eccentricity and hence will be reflected in current spectrum by the following equation:

$$f_{\text{bng}} = |f_e \pm mf_v|, \tag{3}$$

where m = integer $1, 2, 3, \ldots, k/(p/2)$ = integer $1, 5, 7, 11, 13, \ldots$, s = per unit slip and p = number of poles in the induction motor. Slip 's' (given in percentage) can be found out from the following equation:

$$s = \frac{N_s - N}{N_s}100, \tag{4}$$

where N_s and N are synchronous speed and speed of the induction motor, respectively.

In this study of multi-stage synchro-mesh gearbox transmission system, the characteristics frequencies (f_v) are input shaft frequency (f_1), lay shaft frequency (f_2), the output shaft frequency (f_3) and various tooth meshing frequencies (f_{m2}, f_{m3} and f_{m4}) as shown in Fig. 2. Yacamini et al. [21] have derived the effect of a single frequency torsional vibration on the stator current. They have also inferred that high-frequency torsional vibration is being damped by the induction motor. Hence, the effect of torsional vibration only due to rotating frequencies have been considered in this article while deriving the resultant R-phase current, which is an extension of the derivation given in Ref. [21].

The air-gap torque in the induction motor consists of a constant (or average) torque and some oscillatory torques due to torsional vibrations at frequency f_1, f_2 and f_3 with respective phases ϕ_1, ϕ_2 and ϕ_3 given by Eq. (5)

$$T = T_0 + T_1\ \cos(2\pi f_1 t + \phi_1) + T_2\ \cos(2\pi f_2 t + \phi_2) + T_3\ \cos(2\pi f_3 t + \phi_3). \tag{5}$$

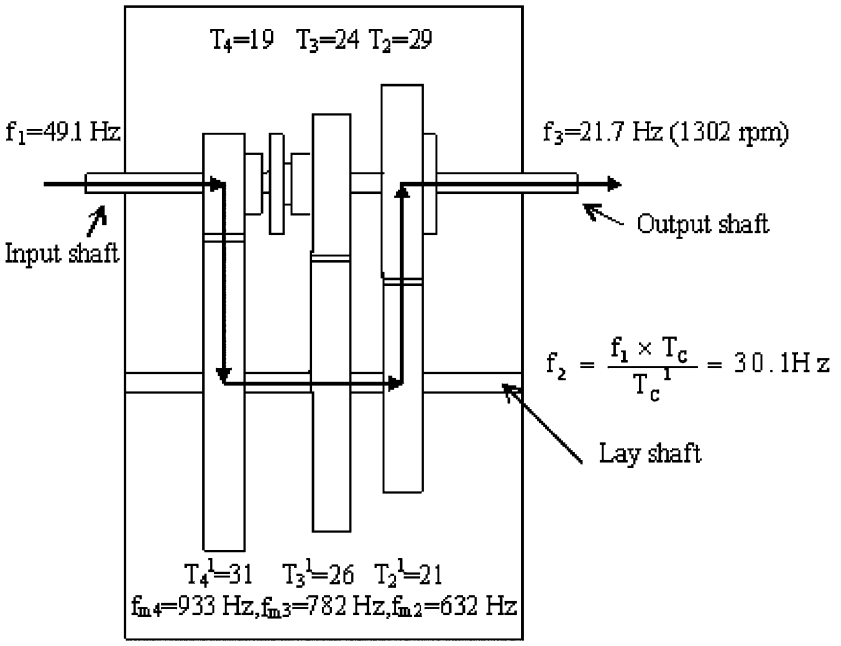

Fig. 2. Line diagram of meshing during 2nd gear operation with 5.625 kW load.

The current will have two components, magnetising current component I_{sM} that is in phase with flux vector; and torque producing component I_{sT} that is 90° ahead of the flux vector. The vector diagram of all the current components is shown in Fig. 3. Due to torsional vibration, these components will also have an average value as I_{sM0} and I_{sT0}, respectively, and oscillating components given in Eq. (6).

$$I_{sM} = I_{sM_0} + A_{sM_1}\sin(2\pi f_1 t + \phi_{M_1}) + A_{sM_2}\sin(2\pi f_2 t + \phi_{M_2}) + A_{sM_3}\sin(2\pi f_3 t + \phi_{M_3}), \tag{6a}$$

$$I_{sT} = I_{sT_0} + A_{sT_1}\cos(2\pi f_1 t + \phi_{T_1}) + A_{sT_2}\cos(2\pi f_2 t + \phi_{T_2}) + A_{sT_3}\cos(2\pi f_3 t + \phi_{T_3}). \tag{6b}$$

The current in any phase; which would have been a pure sinusoidal function, had there been no defects; will be affected by these components. The R-phase current can be given by the following equation:

$$\begin{aligned} I_{sr} &= I_{sM}\sin 2\pi f_e t + I_{sT}\cos 2\pi f_e t \\ &= [I_{sM_0} + A_{sM_1}\sin(2\pi f_1 t + \phi_{M_1}) + A_{sM_2}\sin(2\pi f_2 t + \phi_{M_2}) \\ &\quad + A_{sM_3}\sin(2\pi f_3 t + \phi_{M_3})]\sin 2\pi f_e t \\ &\quad + [I_{sT_0} + A_{sT_1}\cos(2\pi f_1 t + \phi_{T_1}) + A_{sT_2}\cos(2\pi f_2 t + \phi_{T_2}) \\ &\quad + A_{sT_3}\cos(2\pi f_3 t + \phi_{T_3})]\cos 2\pi f_e t. \end{aligned} \tag{7}$$

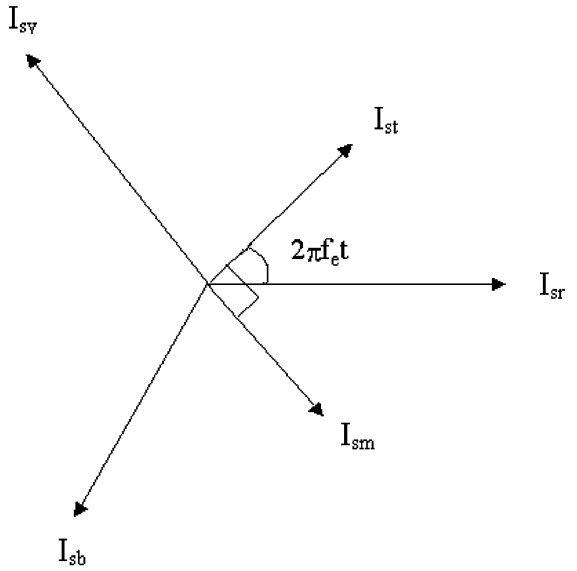

Fig. 3. Vector diagram of all current components in the induction motor.

Simplifying the above equation,

$$
\begin{aligned}
I_{sr} = {} & I_0 \sin(\sin 2\pi f_e t + \phi_0) \\
& + \left(\frac{A_{sT_1} + A_{sM_1}}{2}\right) \cos(2\pi(f_e - f_1)t - \phi_{M_1}) + \left(\frac{A_{sT_1} - A_{sM_1}}{2}\right) \cos(2\pi(f_e + f_1)t + \phi_{M_1}) \\
& + \left(\frac{A_{sT_2} + A_{sM_2}}{2}\right) \cos(2\pi(f_e - f_2)t - \phi_{M_2}) + \left(\frac{A_{sT_2} - A_{sM_2}}{2}\right) \cos(2\pi(f_e + f_2)t + \phi_{M_2}) \\
& + \left(\frac{A_{sT_3} + A_{sM_3}}{2}\right) \cos(2\pi(f_e - f_3)t - \phi_{M_3}) + \left(\frac{A_{sT_3} - A_{sM_3}}{2}\right) \cos(2\pi(f_e + f_3)t + \phi_{M_3}),
\end{aligned}
\tag{8}
$$

where $I_{sM} = I_0 \cos\phi_0$; $I_{sT} = I_0 \sin\phi_0$ and $\phi_0 = \tan^{-1} I_{sT}/I_{sM}$.

The result indicates that any torsional vibration with a specific frequency will have sidebands across the supply line frequency in the motor current signature. Here it has been assumed that $\phi_M \cong \phi_T$.

Similarly, the Y-phase current and B-phase current can be expressed by Eq. (9).

$$
I_{sY} = I_{sM} \sin\left(2\pi f_e t - \frac{2\pi}{3}\right) + I_{sT} \cos\left(2\pi f_e t - \frac{2\pi}{3}\right) \tag{9a}
$$

and

$$
I_{sB} = I_{sM} \sin\left(2\pi f_e t + \frac{2\pi}{3}\right) + I_{sT} \cos\left(2\pi f_e t + \frac{2\pi}{3}\right). \tag{9b}
$$

2.2. Wavelet transform

Wavelet transform can mainly be applied in two ways: DWT and CWT. In DWT, the signal is decomposed into two frequency bands, the lower-frequency band is known as approximate level (A) and the higher-frequency band (octave) is known as detail level (D). For a multi-resolution DWT, a tree can be formed where the signal can be decomposed to a number of octave details and one approximate. Fig. 4 is an example of such decomposition and the equation that governs this is as follows [14,24]:

$$f_J(t) = \sum_{j=J_0}^{J-1} \sum_k \gamma_{j,k} \psi_{j,k}(t) + \sum_k \lambda_{J_0,k} \phi_{J_0,k}(t), \tag{10}$$

where $f_J(t)$ denotes the signal, the first and second part denotes details and approximate levels, respectively, j- and k signify the level and data translation, respectively. The number of decomposition level is $(J-J_0)$. $\psi(t)$ and $\phi(t)$ are the wavelet and scale function, respectively; and γ and λ are the respective coefficients of these functions. The maximum number of decomposition level depends on the number of data points taken. Fig. 1(a) and (b) show the scale and wavelet function of mother wavelet 'D8' used in this article.

CWT considers dilation and translation factors for continuous time and time-scale parameter; and is governed by the following equation [25]:

$$CWT(a,b) = \frac{1}{\sqrt{|a|}} \int_{-\infty}^{\infty} f(t) \psi^* \left(\frac{t-b}{a} \right) \mathrm{d}t, \tag{11}$$

where 'a' is the dilation factor or scale index (inversely proportional to frequency) given by 2^j and 'b' is the time shifting or data translation factor given by $2^j k$. In case of DWT, 'a' and 'b' have specific integer values of j and k, respectively, $\psi^*(t)$ is the complex conjugation of $\psi(t)$. CWT coefficients are complex in nature with modulus and phase. Hence squaring of the coefficients is necessary in order to represent the energy level possessed in a signal and such a plot is known as scalogram.

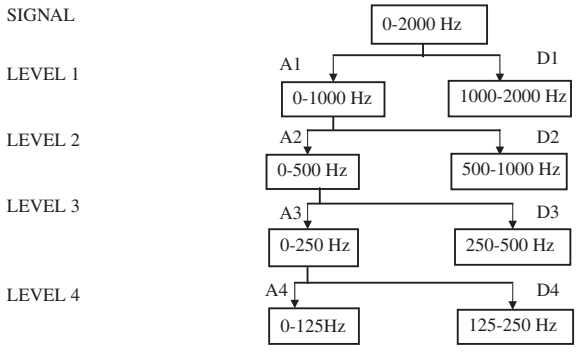

Fig. 4. DWT tree for decomposition of steady signals within 2 kHz for analysing combined DWT and FFT analysis.

3. Experimental procedure

3.1. Gearbox experimental set-up

The experimental set up consists of a two-pole three-phase induction motor coupled to a 4-speed automobile gearbox. The output shaft of the gearbox is connected to a separately excited D.C. generator by a constant-velocity joint. The armature of the D.C. generator was connected to a 5.625 kW variable resistance load. By varying the resistance load with the help of electrical switches, the load on the gearbox could be changed as and when required. The three-phase induction motor was of 7.5 kW capacity and the separately excited D.C. generator had a power output of 5.625 kW. The four-speed transmission gearbox has 2nd, 3rd and 4th gears as synchro-meshed gears and crash type, 1st and reverse gears. The detail specification of the transmission gearbox is shown in Table 1. The input speed of gearbox is the mechanical speed of induction motor (frequency f_1). The lay shaft speed (f_2) and the tooth meshing frequencies can be calculated by using Eq. (12). This study was kept limited to 2nd gear operation for which tooth meshing due to 1st gear has not been considered. The line diagram of the gear meshing is shown in Fig. 2. The expressions for different frequencies are given in the following equation:

$$f_2 = 0.6129 f_1; \quad f_{m2} = 21 f_2; \quad f_{m3} = 26 f_2 \text{ and } f_{m4} = 31 f_2 \tag{12}$$

where f_{m2}, f_{m3} and f_{m4} are tooth-meshing frequencies corresponding to 2nd gear, 3rd gear and 4th gear, respectively. The output shaft frequency (f_3) depends purely on f_1 and the gear ratio. For different gear operation, f_3 can be calculated by the following relationships:

$$f_3^2 = f_1/2.253; \quad f_3^3 = f_1/1.506; \text{ and } f_3^4 = f_1. \tag{13}$$

To study the effect of faults in gears, defects are introduced artificially in the 2nd gear. In the first case, one tooth of the 2nd gear in the main shaft was removed and in the second case, two teeth of the same gear were removed, by using die-sinking electro-discharge machining (EDM). Figs. 5(a) and (b) shows gears in the first and second cases (referred as defect-1 and defect-2 in this article), respectively.

In the synchro-mesh gearbox, vibration and motor current signatures were acquired while the gearbox was operating in the second gear. To measure the gearbox vibration, a B&K 4370 accelerometer was stud mounted near the tail-end bearing of the gearbox casing. A B&K 2632 NEXUS charge amplifier was used to condition the accelerometer signal.

For measuring the input current waveform of the three phases of the induction motor, 3 numbers of Tektronix A622 hall effect current probes were used. The output from the

Table 1
The specification of gear transmission system

Items	2nd gear	3rd gear	4th gear
No. of teeth (in main shaft)	29	24	19
No. of teeth (in lay shaft)	21	26	31

Fig. 5. (a) One tooth broken in the 2nd gear (defect-1), (b) Two teeth broken in 2nd gear (defect-2).

accelerometer and the current probes were recorded in an 8-channel DAT recorder (SONY PC 208 Ax). The rotation speed of the motor was measured with a B&K MM0024 photo-electric probe.

3.2. Analysis techniques

FFT analysis is used for the correlation of the vibration signatures and current signatures. But due to several demerits of the FFT analysis such as inability to analyse transients, inability to detect time of discontinuity etc., time-scale or time–frequency methods are required to analyse the current and vibration signals. There are already a number of literatures available citing the advantages of time-scale methods such as wavelet transform over time–frequency methods such as

WVD and STFT [15–18]. Application of WVD gives rise to cross terms whereas in STFT, the uncertainty principle [14] limits the resolution of the time and frequency. Moreover, the choice of window size hampers the result greatly in STFT. In this paper, the following techniques are applied:

1. FFT technique for low-frequency (0–100 Hz) and high-frequency (0–1000 Hz) analysis of current and vibration signals.
2. Decomposition of current signal (upto 2 kHz) using discrete wavelet technique, and then FFT analysis of details 'D2'. This detail level 'D2' (500–1000 Hz) shown in Fig. 4, contains the sidebands of the gear meshing frequencies across the supply line frequency.
3. DWT and CWT to transients of signal due to load fluctuation.

3.3. Data acquisition methodology

The investigation of spectrum of the signals was carried out with two frequency ranges such as a low-frequency range of 0–100 Hz and a high-frequency range of 0–1000 Hz. The low-frequency range revealed the different rotational frequencies, for which signal was extracted with a 200 Hz sampling frequency and 1024 numbers of data points. To study the higher-frequency range (0–1 kHz) that carries details of the tooth-meshing frequencies, 8192 numbers of data were extracted with a sampling frequency of 4.096 kHz and 2 s time record. Signals were acquired on a personal computer through an (NationaI Instruments 6110 E) analog-to-digital conversion card after passing the signal through an analog low-pass filter (Stanford Research Systems SR650) anti-aliasing filter of 100 Hz and 2 kHz, respectively, for the two cases of analysis.

The same high-frequency steady current signals (within 2 kHz) have been used for decomposition using DWT. All the steps were repeated for several steady load conditions. The load conditions were 5.625, 3.75, 1.875 and 0 kW.

To study the transients of MCSA, current signatures were acquired on a personal computer through the above-mentioned A/D card after passing through a low-pass filter of 10 kHz. The sampling frequency was 20.48 kHz and numbers of data points taken were 8192 resulting in a time record of 0.4 s. Three numbers of load fluctuation cases are discussed. These are 5.625 kW to no load, 3.75 kW to no load, and 1.875 kW to no load.

4. Results and analysis

4.1. FFT analysis of current and vibration signals

Fig. 6 shows the spectra of the steady vibration signatures and current signatures of the gearbox with no defect, one defect in the 2nd gear (defect-1) and two defects in the 2nd gear (defect-2) at 5.625 kW load condition, within the frequency range 0–100 Hz. The spectra of all other load conditions such as 3.75, 1.875 and 0 kW has also been studied and the summary of the results is plotted in Fig. 7. The following observations are made:

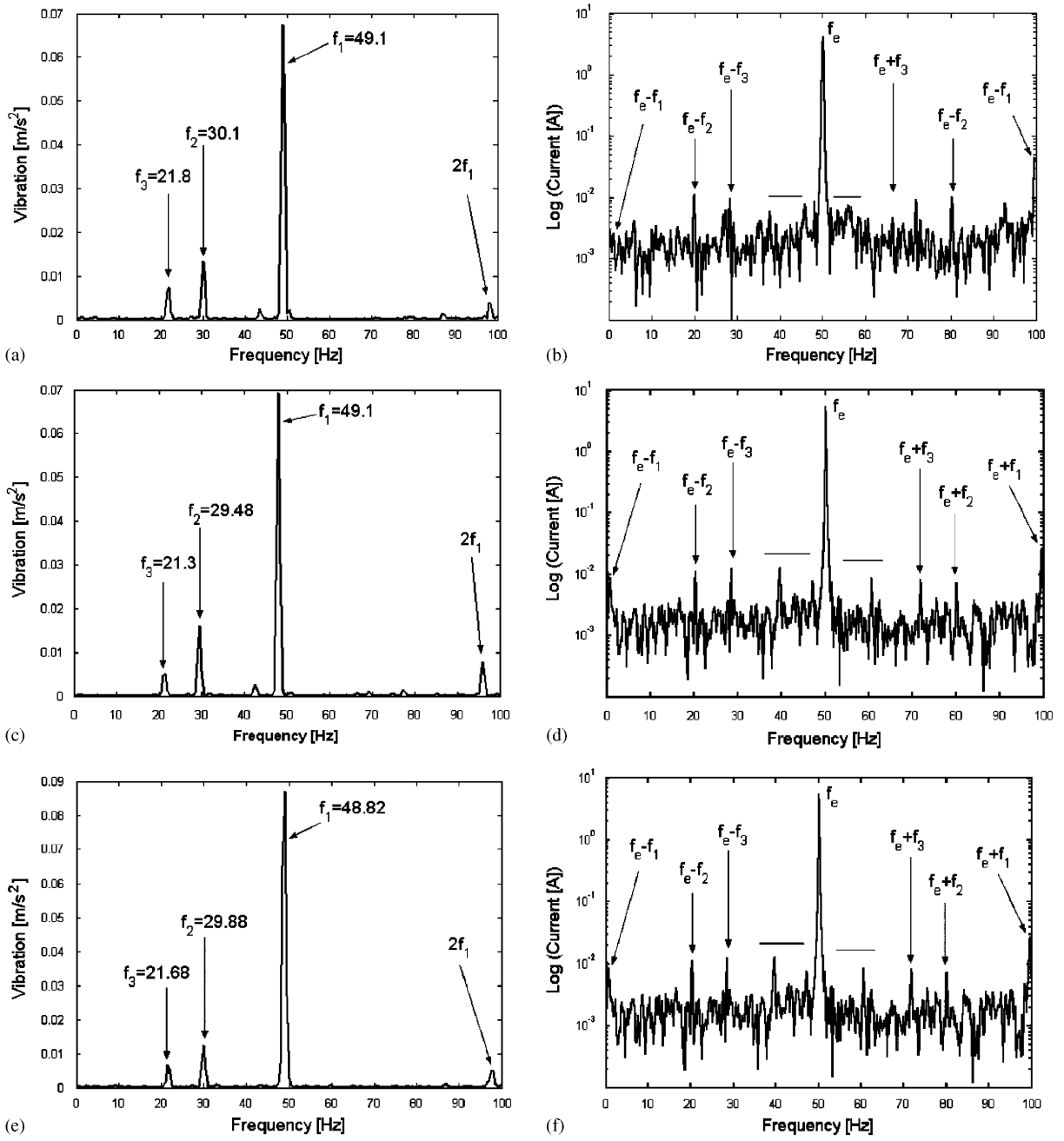

Fig. 6. Spectra of vibration and current signatures (0–100 Hz) at 5.625 kW load condition with no defects: (a, b); defect-1: (c, d); and defect-2: (e, f).

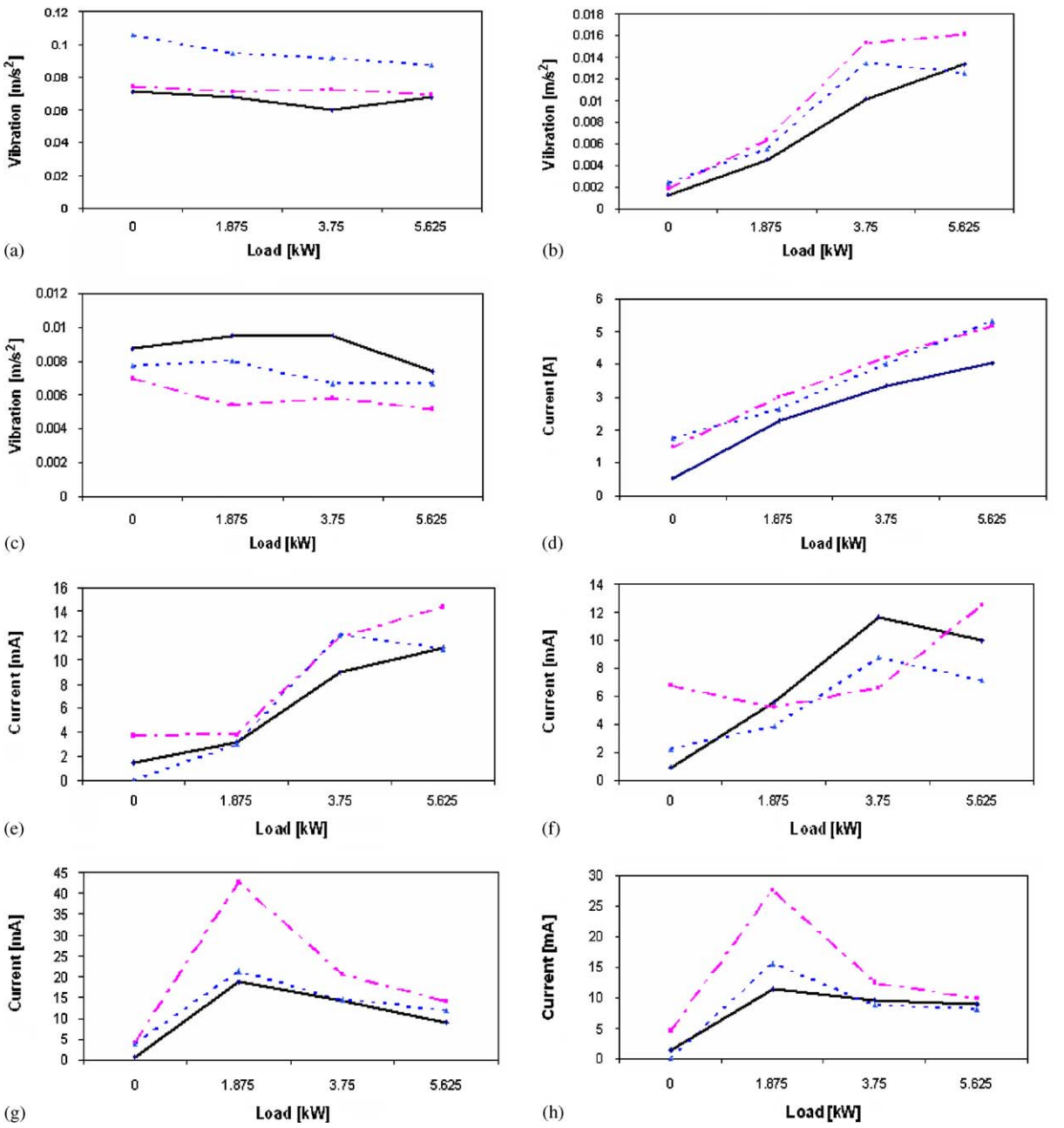

Fig. 7. Summary of FFT analysis of vibration and current signatures within 0–100 Hz for following frequencies. (a) f_1; (b) f_2; (c) f_3; (d) f_e; (e) f_e-f_2; (f) f_e+f_2; (g) f_e-f_3; and (h) f_e+f_3. –●–, No Defect; —■ -, Defect-1; - ▲ -, Defect-2.

1. The rotating shaft frequencies such as input shaft frequency (f_1), lay shaft frequency (f_2) and output shaft frequency (f_3) are of the order of 49, 30 and 20 Hz, respectively, and hence lie within 0–100 Hz range. In all the vibration spectra, prominent frequencies such as f_1, f_2, f_3 are

observed. In some cases, harmonics of f_1 and f_3 are also detected. The corresponding sidebands of the rotating frequencies across the line frequency (f_e) are observed in the current spectra.

2. Rotor eccentricity in the induction motor governed by Eq (1) is also traced by examining the remaining sidebands of the line frequency in the current signatures. These are shown by a line drawn in the spectra. Since, the amount of load affects the rotor speed, the slip factor also changes in each case. The amplitudes of the sidebands due to rotor eccentricity are very large after the load removal than those before the load removal. It is due to the fact that the load acts as a damping factor for vibrations due to the rotor eccentricity [18].
3. In an induction motor, the speed is inversely related with the load, however when it is coupled with a gearbox, a large fluctuation of speed of the order of 0.5 Hz (30 rpm) is observed. For example, it has been observed that a defect-free gear running at 3.75 kW load has input shaft speed of 49.7 rpm whereas at 1.875 kW, it is 49.4 rpm. The reason is that the gearbox casing vibration is retransmitted to the gearbox through flexible rolling element bearing, and very large excitation of the gearbox takes place due to various time-varying parameters like tooth mesh stiffness, frictional forces and torques and bearing forces; thereby causing a large speed fluctuation [26]. Hence, tracking of the rotating speed is not effective in monitoring of the gearbox.
4. The changes in amplitudes at input shaft frequency in vibration signatures (Fig. 7(a)) with load is more consistent, so is the case for the supply line frequency (f_e) (Fig. 7(d)) and its left-hand sidebands of lays shaft frequency in the MCSA (f_e-f_2) (Fig. 7(e)). The layshaft frequency (Fig. 7(b)) can be useful in detecting defects at low loads. All other components vary arbitrarily with load. But for detecting defects, along with these frequencies, input frequency in the vibration signature (f_1) (Fig. 7(a)) and left-hand sideband of output frequency (f_e-f_3) (Fig. 7(g)) can be focused.

Fig. 8 depicts the spectra of vibration signatures and corresponding current spectra within 0–1000 Hz range for no defect, defect-1 and defect-2 at a load of 5.625 kW. This frequency range is very vital for studying the transmission gearbox as all the tooth-meshing frequencies generally fall within this frequency of 0–1000 Hz range. The tooth/gear meshing frequencies for 2nd, 3rd and 4th gear pairs are of the order of 630, 780 and 940 Hz, respectively. These vary widely with the load fluctuation. The vibration spectra for all other load conditions are studied and the summary is plotted in Fig. 9. The following observations are made:

1. In the vibration signatures of all the four steady load conditions, it is observed that the amplitude of the tooth/gear mesh frequencies (GMFs) are very large in comparison to that of the shaft frequencies and there are sidebands of these shaft frequencies across the GMFs. But levels of amplitude of these GMFs and the number of sidebands gradually reduce with the decrease in load. The current spectra possess sidebands of these GMFs across the line frequency. But the amplitude levels of these sidebands are very low in comparison to the amplitude levels of line frequency and its harmonics resulting in a false notion that the MCSA may not be well suited to study higher-frequency ranges while being very efficient in detecting the lower-frequency ranges of the vibration signature. The same inference has been drawn by Yacamini et al. [21] that high-frequency vibrations are damped in induction motors.

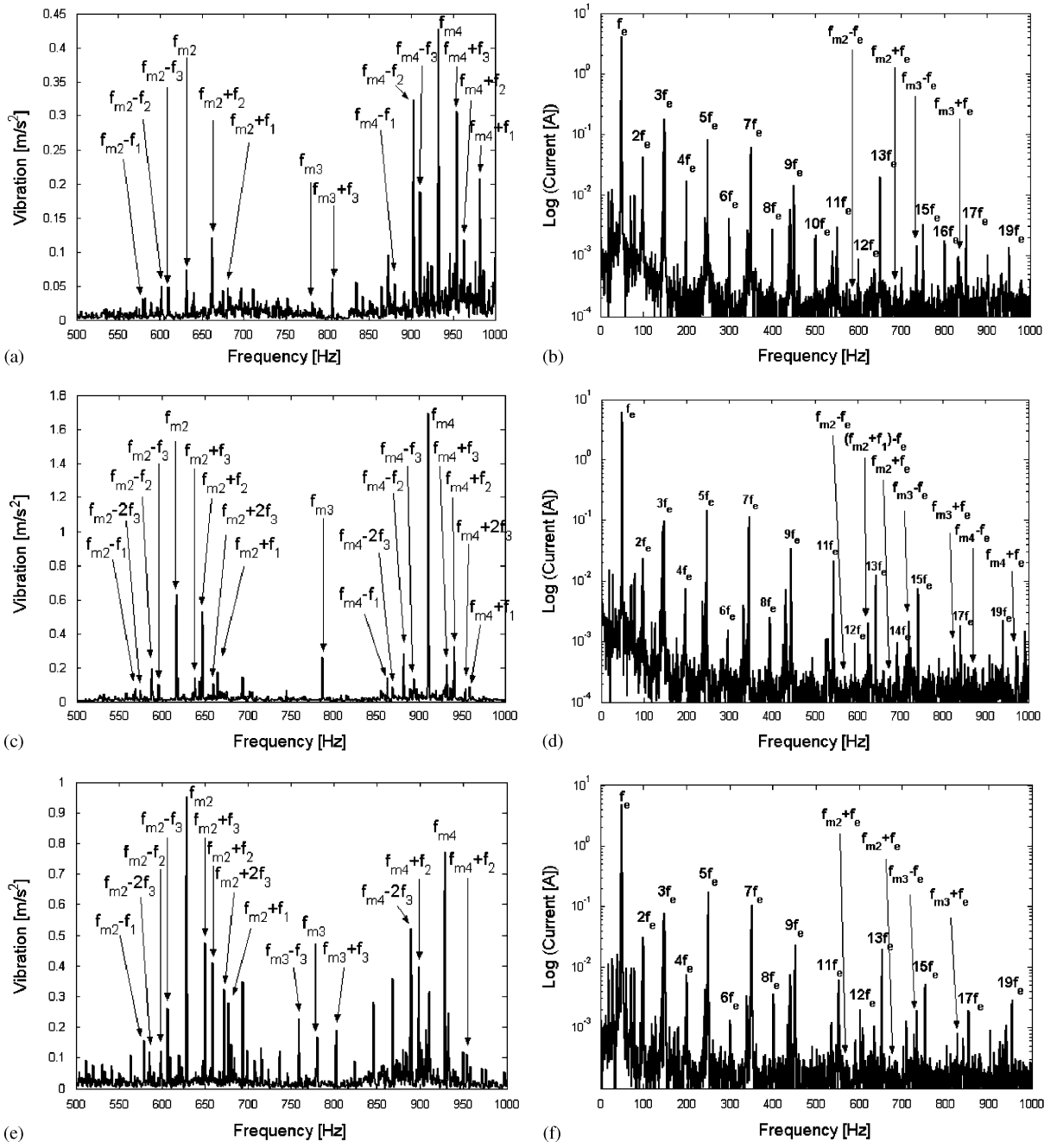

Fig. 8. Spectra of vibration and current signatures (0–1000 Hz) at 5.625 kW load for various defect conditions, with (a,b) no defects; (c,d) defect-1; and (e,f) defect-2.

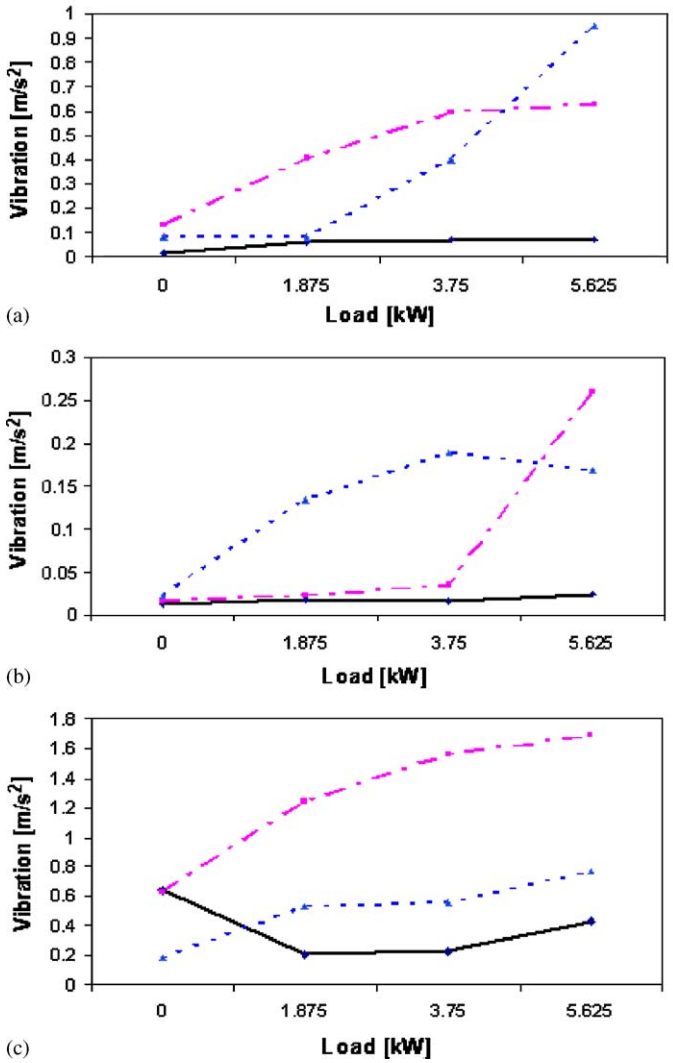

Fig. 9. Summary of the important components of vibration for the following frequencies; (a) 2nd GMF (f_{m2}), (b) 3rd GMF (f_{m3}) and (c) 4th GMF (f_{m4}). –●–, No Defect; —■ -, Defect-1; - ▲ -, Defect-2.

2. Fig. 9 indicates that 2nd GMFs have very high vibration due to defects in 2nd gear. But in the 4th GMF, the case of defect-1 has more vibration than the other cases that gradually decreases with load fluctuation. The reason is that vibration generally occurs because of gear backlash and tooth stiffness variation [27]. Backlash is much more for the case of two teeth broken than the case of one tooth broken. Hence the severity of vibration of two teeth broken is less than that of one tooth broken. The severity of vibration is so much that signatures also contains sidebands of harmonics of rotating frequencies at 2nd GMF. But in the no load condition, the 4th GMF has very high vibration, due to the fact that load acts as damper. The vibration of 3rd

GMF (with a maximum vibration of 0.26 m/s^2) (Fig. 9b) is comparatively much less than the others as it rotates freely because of synchro-mesh condition, while the other gears transmit power when the gearbox is operating in 2nd gear.

4.2. Combined DWT and FFT analysis of steady current signals

DWT decomposes a signal into one approximate and several details levels depending upon the number of decompositions. The level of decomposition is important, as it should investigate all the component frequencies present in the signal, but is limited by the number of data points taken. In this section, DWT is applied to steady current signals with a maximum frequency content of 2 kHz.

Fig. 4 shows the decomposition of steady current signals to 4 levels with the frequency content of each level. The decomposed signals for defect-1 condition at 5.625 kW load is shown in Fig. 10. For all other load conditions and cases of no defect and defect-2, signals are decomposed. Out of these decomposed signals, details at 2nd level (D2) is an important level of consideration which has a bandwidth of 500–1000 Hz containing the sidebands of GMFs across supply line frequency (f_e). FFT analysis is applied to this D2 level-decomposed signal in order to detect these frequencies. The advantage of this methodology is that

1. the signal will have a high signal to noise ratio at high frequencies;
2. absence of supply line frequency and its near harmonics (contained mainly in approximate 4 (A4) and detail 4 (D4) will result in zooming of the sidebands of the GMFs across the supply line frequency. It has been observed that even a frequency with very small amplitude of 1 mA of the current signal can be monitored easily using such an analysis.

The results of this FFT analysis of D2 signals for no defect, defect-1 and defect-2 at 5.625 and 0 kW load conditions are shown in Fig. 11, respectively. After studying the remaining load conditions of 3.75 and 1.875 kW, the results are summarized in Fig. 12. The observations are as follows:

1. The sidebands of the gear mesh frequencies particularly pertaining to f_{m2} and f_{m3} across supply line frequency f_e are observed. Even, this methodology is able to detect the sidebands of rotating shafts across GMFs observed in frequency-domain signatures of vibration shown in Fig. 8. The amplitudes of these sidebands are found to be around 10 mA, which are considerably less than the amplitude of the supply line frequency (which is in the order of 1–6 A). This is the reason, that in the conventional FFT analysis, these components were difficult to be detected. But combination of DWT and FFT analysis is a powerful technique that can detect these sidebands with very low amplitude.
2. In Fig. 12, it can be seen that defect-1 causes more vibration than defect-2 that has already been conformed in the previous section. It has been observed that the tracking the amplitude of left hand sideband of f_{m2} across supply line frequency i.e. $f_{m2}-f_e$ (Fig. 12(a)) at full load will be the most effective in monitoring defects in the 2nd gear. Other sideband $f_{m2}+fe$ (Fig. 12(b)) may be able to detect defects at all load conditions, but it is difficult to distinguish defect-1 and defect-2 at 5.625 kW load condition. It is a better idea to monitor both the sidebands simultaneously. It

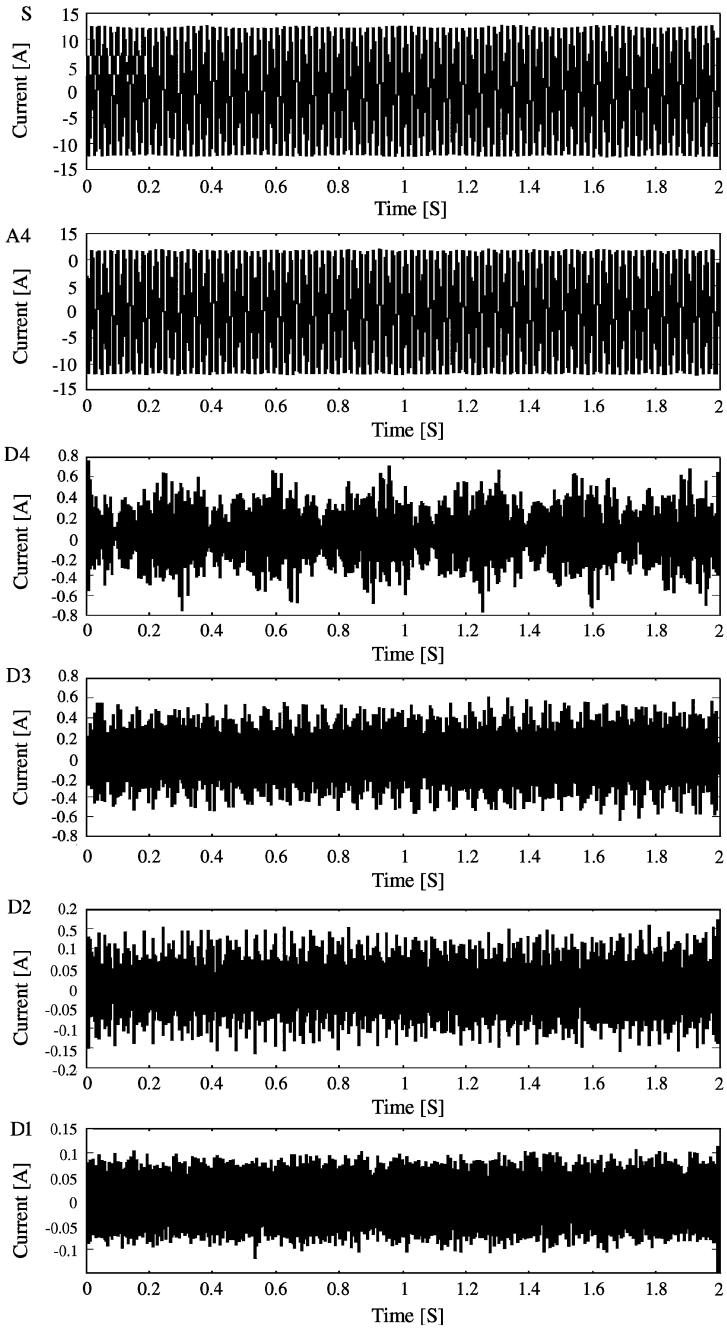

Fig. 10. DWT decomposition of steady current signals (within 2 kHz) for 5.625 kW load and one defect in 2nd gear (defect-1) up to 4 levels beginning from signal, approximate at 4th level and details at 4th level to details at 1st level.

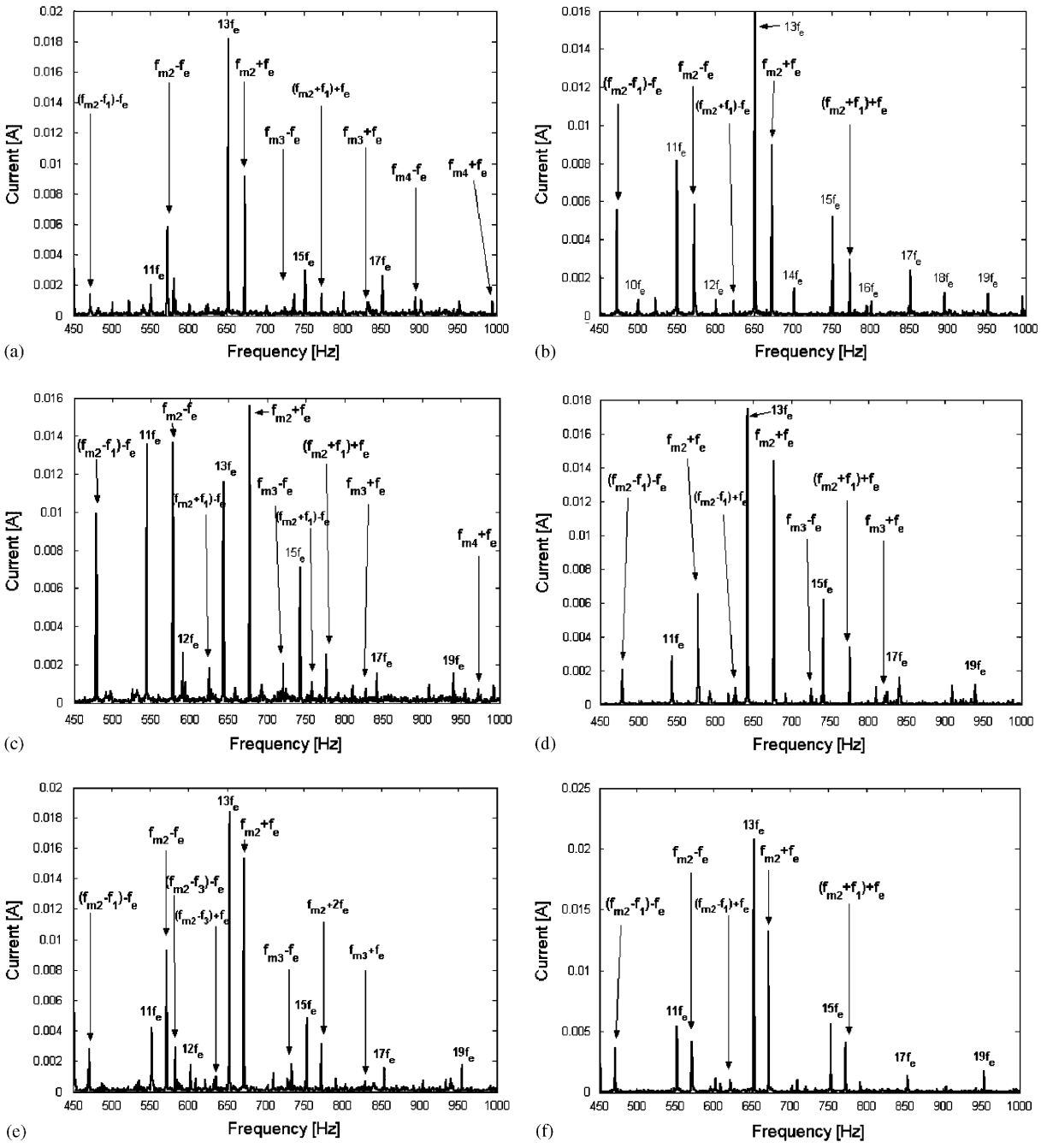

Fig. 11. The FFT analysis of details D2 of the decomposed steady current signals for (a) no defect and 5.625 kW; (b) no defect and 0 kW; (c) defect-1 and 5.625 kW; (d) defect-1 and 0 kW; (e) defect-2 and 5.625 kW; and (f) defect-2 and 0 kW.

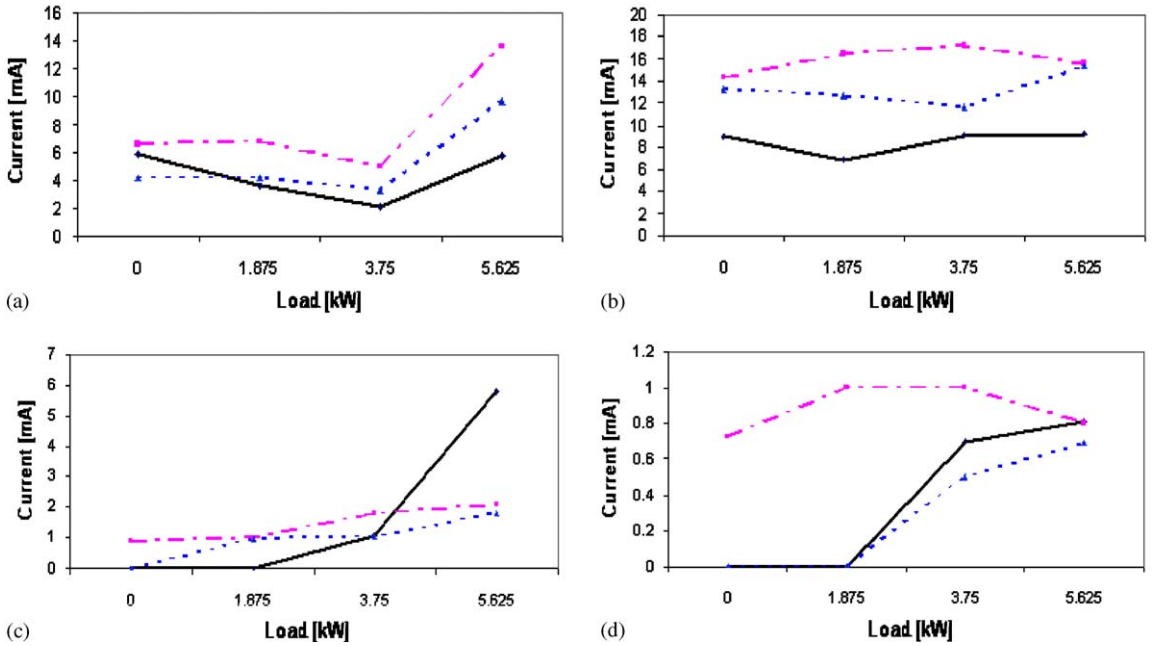

Fig. 12. Summary of the FFT analysis of D2 signals, depicting the amplitude variation of some important components with variation in load and defects; (a) $f_{m2}-f_e$, (b) $f_{m2}+f_e$, (c) $f_{m3}-f_e$, and (d) $f_{m3}+f_e$. –●–, No Defect; —■ -, Defect-1; - ▲ -, Defect-2.

can be noted that monitoring the sidebands of 3rd GMFs across f_e (Fig. 12(c) and (d)) for defects in 2nd gear is not fruitful.

4.3. DWT for current transients

From Fig. 11, an important observation can be noted that the amplitudes of some of the sidebands as well as 11th and 13th harmonics of supply line frequency decrease considerably with decrease in load. Hence, a question may arise whether defect can be monitored through transient analysis of the motor current signature. To answer the question, signals within 10 kHz were acquired with a sampling frequency of 20.480 kHz and 8192 data points with a record time of 0.4 s. Three cases of load fluctuations were analysed for all defect conditions discussed earlier. These load fluctuation cases are 5.625 kW to no load, 3.75 kW to no load, and 1.875 kW to no load. DWT is applied up to 10 levels of decomposition. In the DWT tree which is shown in Fig. 13, the last detail D10 covers frequency bandwidth of 9.765–19.53 Hz. The approximate at level 10 (A10) has frequency bandwidth of 0–9.765 Hz. Hence 10 levels are sufficient to cover all the sidebands of rotating frequencies and gear mesh frequencies. But the important levels to be focused are details at level 4 (D4) having a bandwidth of

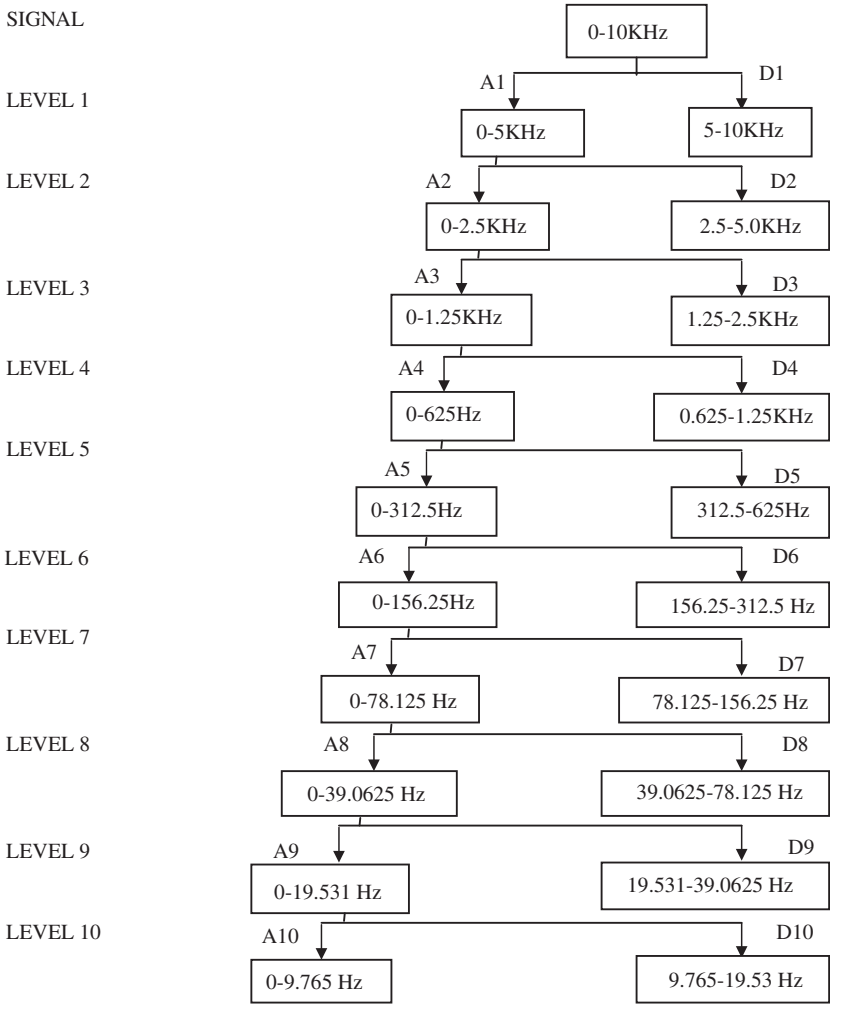

Fig. 13. DWT tree for decomposition of transient current signals within 10 kHz.

625–1250 Hz that accommodates the sidebands of gear mesh frequencies across supply line frequencies, and details at level 3 (D3) which contains harmonics of the components found in D4. The decomposition of the transient current signature with defect-1 and load fluctuation of 5.625 kW to no load is shown in Fig. 14. For all other load fluctuations and defects conditions, decomposition is carried out.

The contour diagrams of the DWT coefficients for all the cases of load fluctuation and defects are shown in Figs. 15(1)–(3). The observations are as follows.

1. The decomposition in Fig. 14 indicates that the transients due to load fluctuation are clearly marked in the level D8, D7, D3 whereas in D4, transient due to defect can be seen.

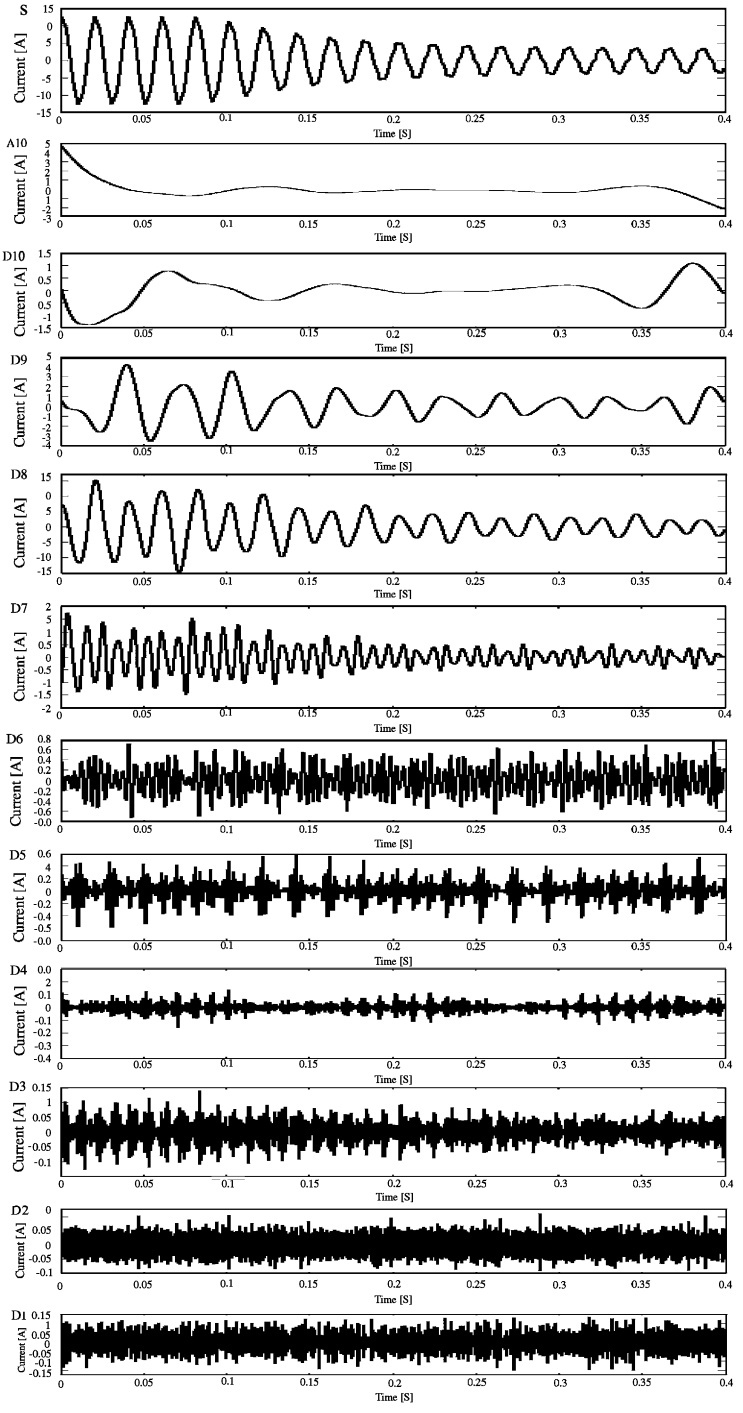

Fig. 14. The DWT decomposition of current transient at 5.625 kW for defect-1 condition beginning from signal, approximate at 10th level, details at 10th level to details at 1st level.

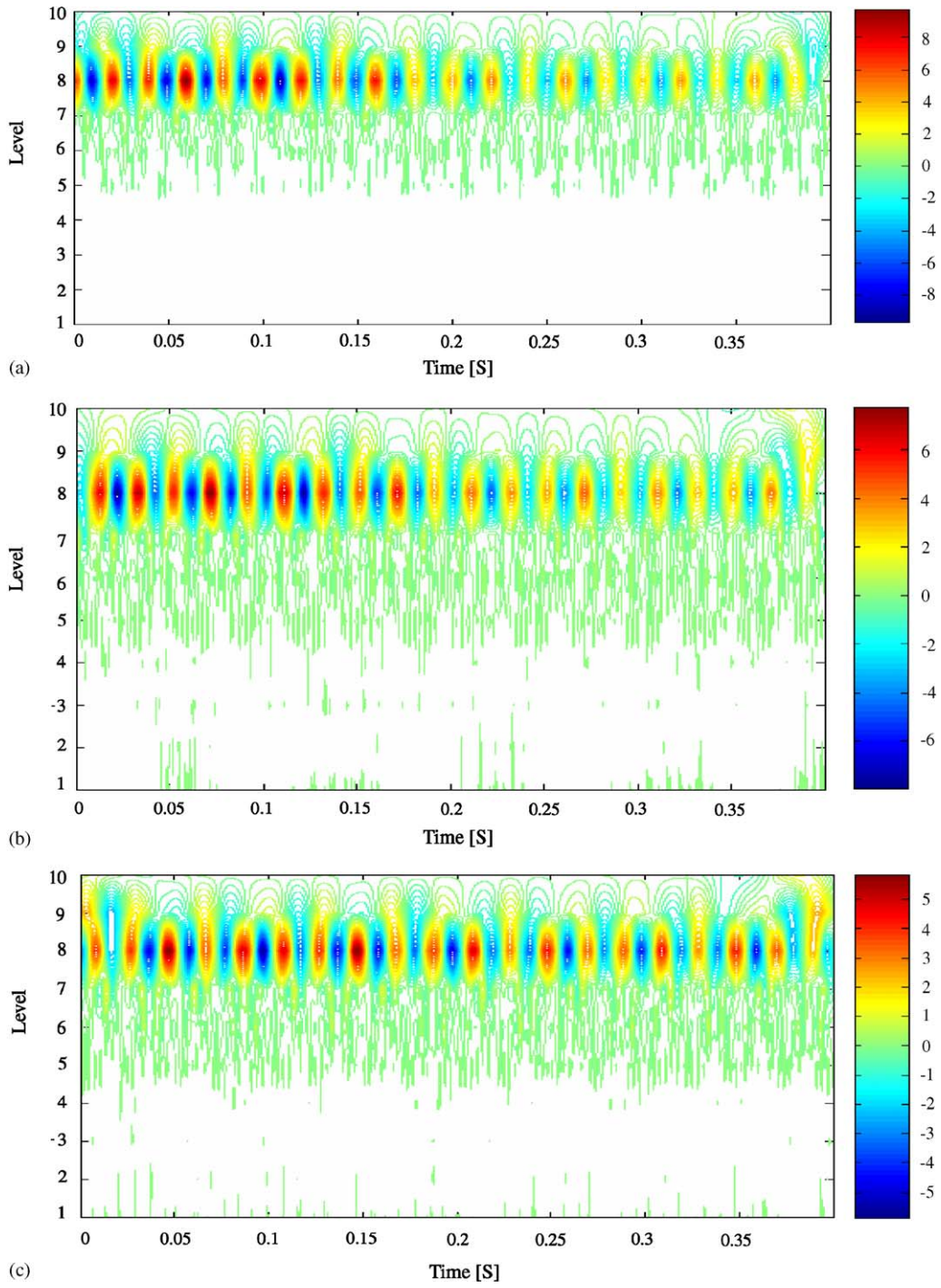

Fig. 15. (1) DWT contour diagrams (with colourbar) of current transients with no defect due to load fluctuation of (a) 5.625–0 kW, (b) 3.75–0 kW and (c) 1.875–0 kW. (2) DWT contour diagrams (with colourbar) of current transients with defect-1 condition due to load fluctuation of (a) 5.625–0 kW, (b) 3.75–0 kW and (c) 1.875–0 kW. (3) DWT contour diagrams (with colourbar) of current transients with defect-2 due to load fluctuation of (a) 5.625–0 kW, (b) 3.75–0 kW and (c) 1.875–0 kW.

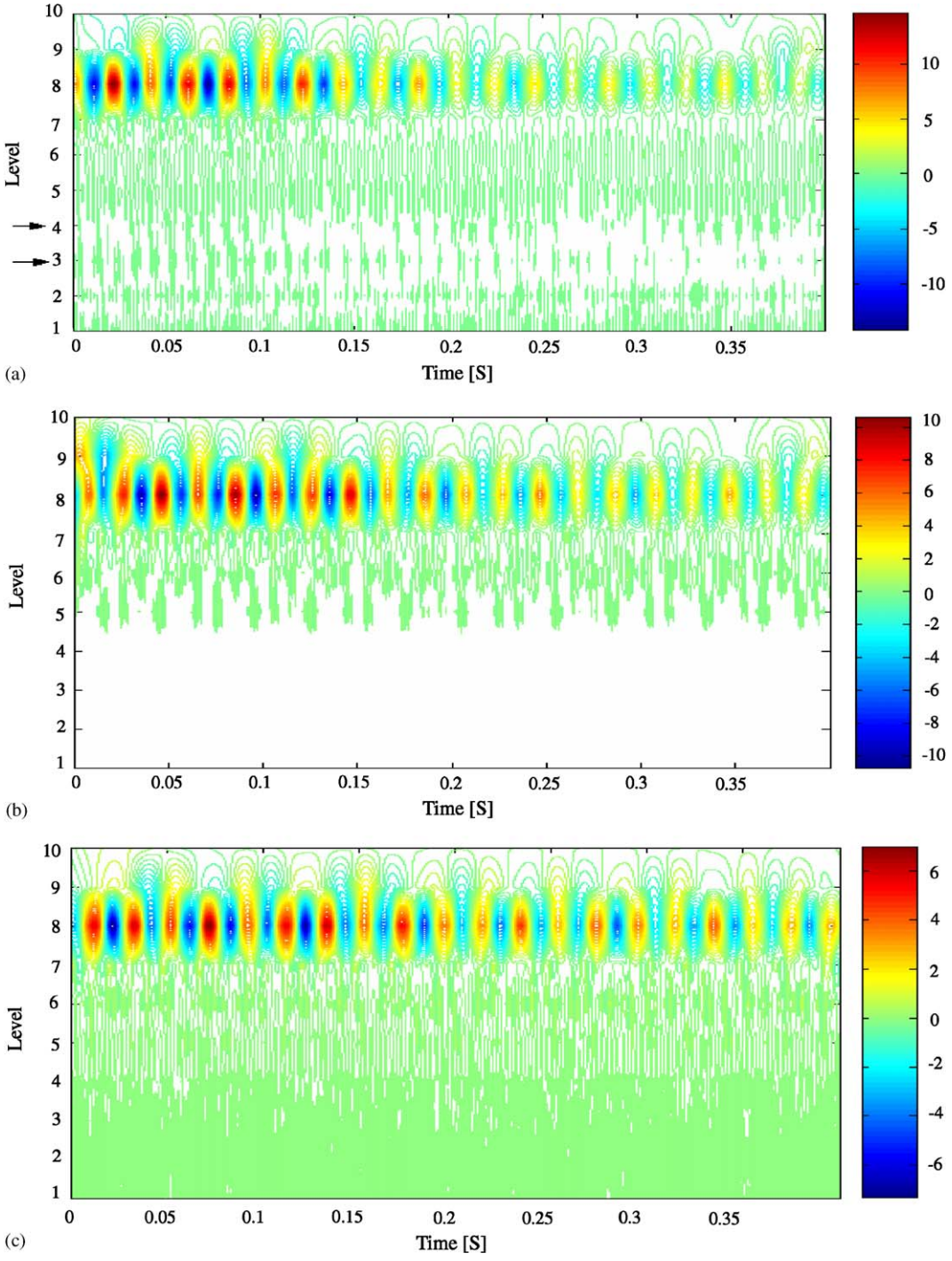

Fig. 15. (*Continued*)

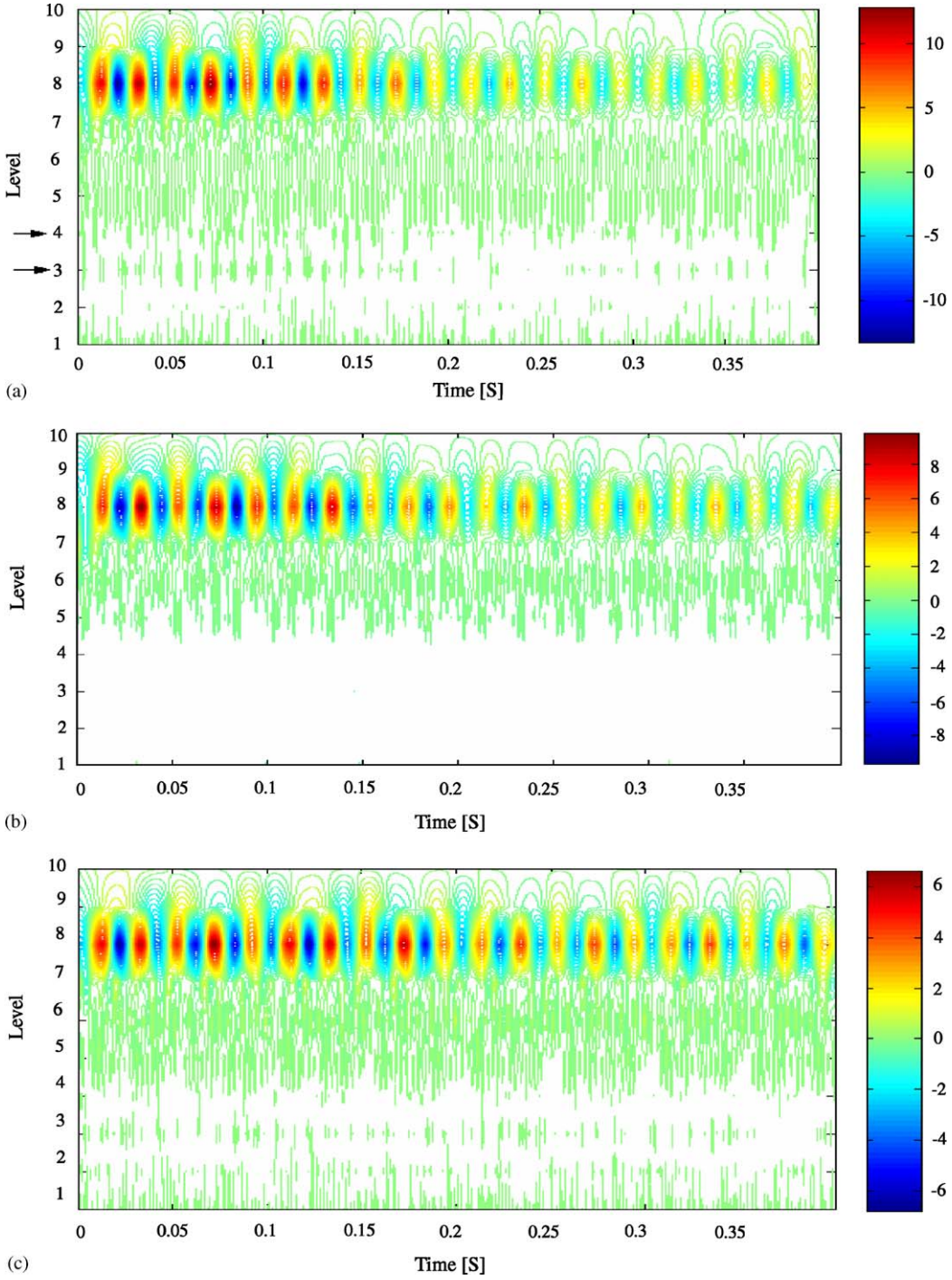

Fig. 15. (*Continued*)

2. The load fluctuation mainly affects the details at 8th level (D8) i.e. the frequency bandwidth of 39–78 Hz, which contains the supply line frequency (f_e) of 50 Hz as shown in Fig. 15.
3. For load fluctuation of 5.625 kW to no load, transients are observed in the region of D3 and D4 (shown by arrows) for both the defective conditions (refer Figs. 15(2a) and 15(3a)), but this transient is absent in the case of no defect and other cases of load fluctuation. The amplitude of this D4 region is of the order of 2 mA (as discussed in previous section), and hence, high resolution is required for which 50 contours are taken in the plots. Hence, it can be inferred that defects in the gearbox can be sensed by imparting very high load fluctuation that will excite the D4 and D3 regions of the decomposed current transients.
4. The magnitudes of the colour bar (in the contour diagrams of all Figs. 15(1)–(3)) corresponds to the amplitude of the resultant signal that matches with the magnitudes of the current signal shown in Figs. 10 and 14. These values can be used to measure the amount of load fluctuation.

4.4. CWT of current transients

CWT with the same mother wavelet 'Db8' is also tried to monitor the defects in 2nd gear. The same data analysed in Section 4.3 is once again analysed. The results are shown in Figs. 16(a–c), for 5.625 kW load fluctuation for no defect and two defective cases, for the load fluctuation case from a load of 5.625 kW to no load. These figures used 50 contours to give the desired resolution. It has been found that the transients due to load fluctuation can be observed centred around the scale of 256–320 (equivalent to within 8th and 9th levels of DWT) whereas transients due to defects are unable to be detected in the scale of 8 and 16 (equivalent to details at 3rd and 4th levels in DWT). The same result has been observed in three-dimensional scalograms shown in Figs. 16(d–f), which are actual indicator of energy transfer in these events where the amplitudes of these scalograms are square of the absolute CWT coefficients. It is inferred that CWT and scalograms are not effective in detecting faults in the transmission system.

5. Conclusions

This article was concerned to study MCSA as a replacement of vibration signature analysis to detect fault and measure load fluctuation. It considered a normal operating transmission gearbox operating at 2nd gear with no defects, one tooth broken in 2nd gear and two teeth broken in 2nd gear. First, the spectra of both vibration signatures and current signatures at four different steady loads are compared. In view of studying higher frequencies of steady current signals, first DWT is applied and then FFT analysis is applied to the details level (D2) that contains the sidebands of gear mesh frequencies across supply line frequency. DWT is also applied to the transients of the current signal due to three different cases of load fluctuation for different defects. CWT is also used in order to detect faults introduced artificially to the 2nd gear. The following inferences are drawn.

1. There are sidebands of the characteristic frequencies of the gearbox; such as rotating frequencies like input shaft, output shaft and lay shaft speeds and gear mesh frequencies like

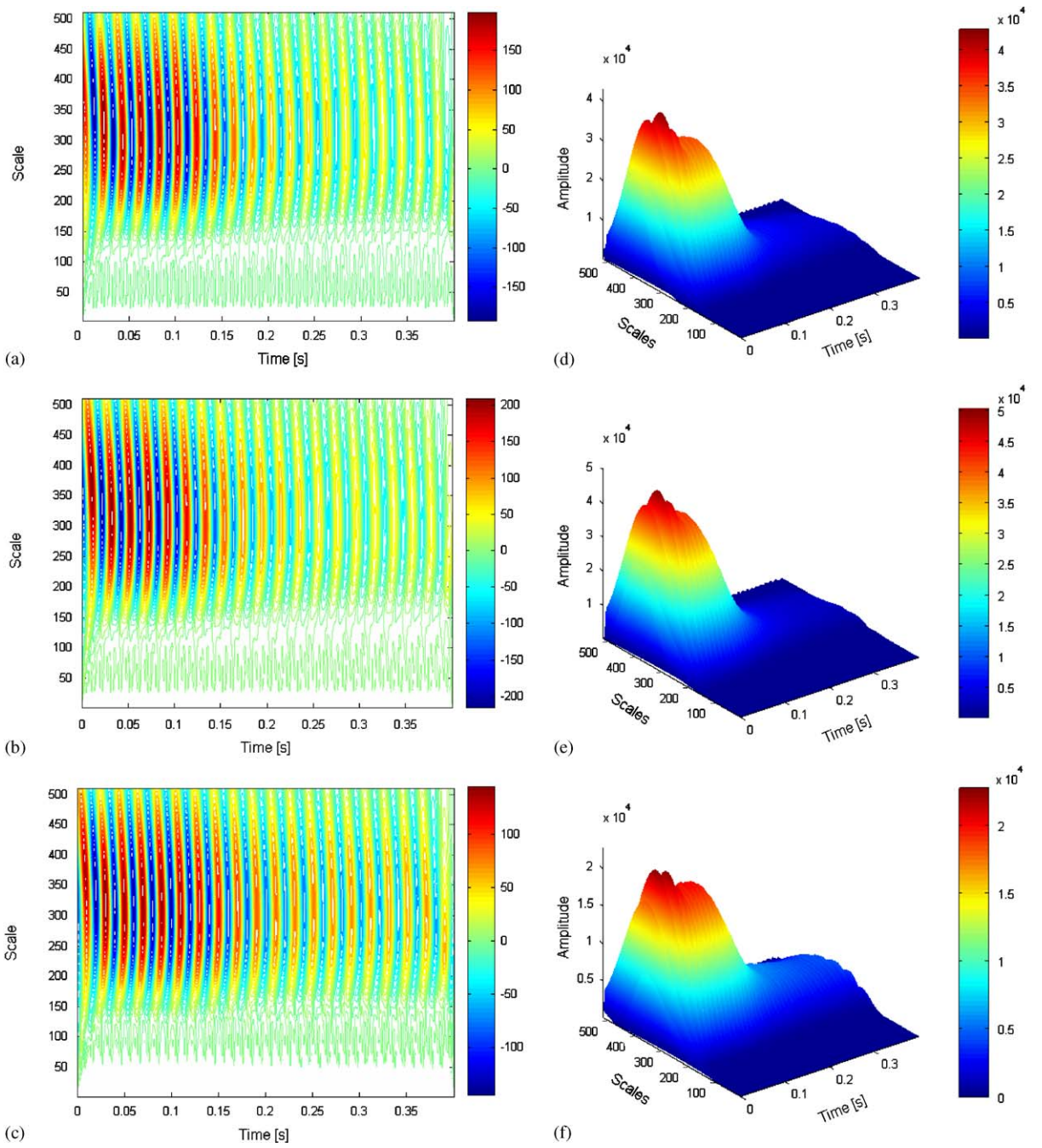

Fig. 16. The CWT coefficient contour plots at 5.625 kW for defect-2, defect-1 and no defect respectively: (a–c); the 3-dimensional Scalograms at 5.625 kW for defect-2, defect-1 and no defect respectively: (d–f).

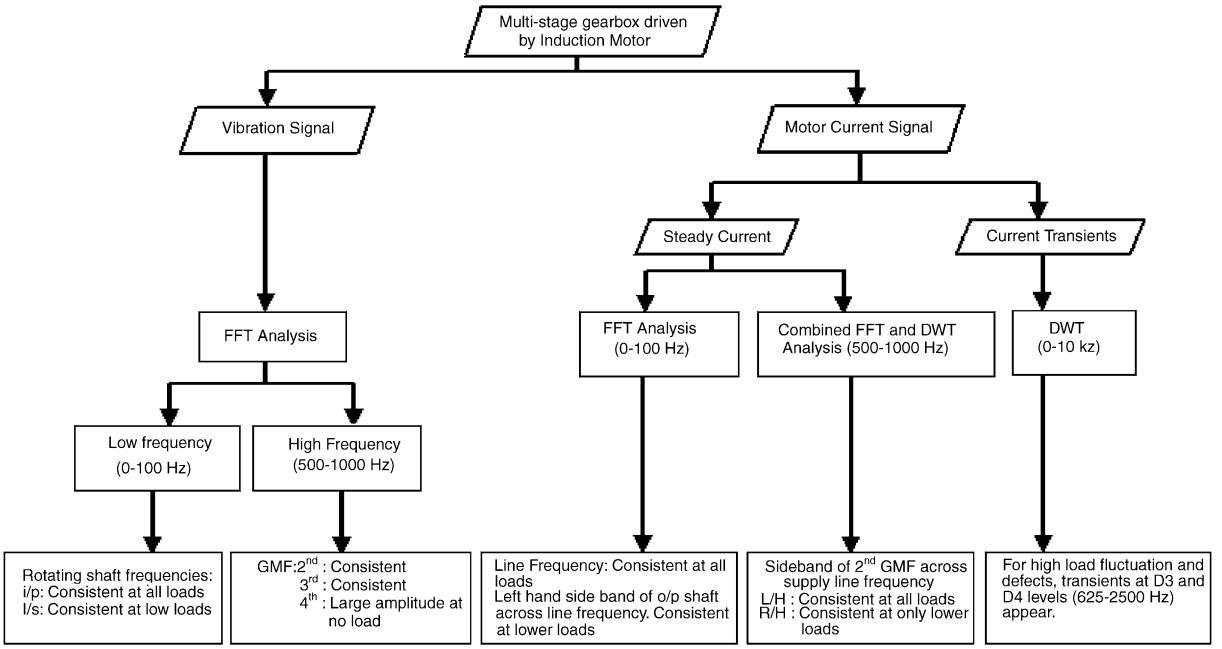

Fig. 17. Decision and diagnostic flow chart for multi-stage gearbox by vibration and current signature analysis.

2nd GMF, 3rd GMF and 4th GMF; across the supply line frequencies in the motor current signature analysis. But these sidebands have very less amplitude compared to the line frequency and its harmonics.

2. The severity of vibration is much more for defect-1 (one tooth broken) than defect-2 (two teeth broken) leading to conclusion that sensing the defects at an early stage will be easier.
3. DWT is much more effective than the CWT and scalogram in detecting faults in the gearbox.
4. Defects and load fluctuation of the multi-stage gearbox can be monitored through motor current signature by
   a. Tracking the amplitude levels of the supply line frequency (f_e) and the left-hand sideband of lay shaft frequency across supply line frequency ($f_e - f_2$) using FFT analysis;
   b. Tracing the sidebands of 2nd GMF across supply line frequency ($f_{m2} - f_e$) and ($f_{m2} + f_e$) using combined DWT and FFT analysis;
   c. Detecting transients at D4 and D3 levels in the DWT contour diagram of the current transients with high gear load fluctuation.

A decision flow chart depicting the processes or techniques adopted and the corresponding decisions is illustrated in Fig. 17. In case of vibration signature analysis, f_1, f_{m2} and f_{m3}; and in case of current signature analysis, f_e and $f_{m2} + f_e$ are consistent in diagnosing faults at any load conditions. This study is limited to only the detection of faults in 2nd gear at 2nd gear operation. There is immense scope of extending this study to detect faults in other gears at different gear

operation. An expert system may well be devised for on-line condition monitoring of the multi-stage gearbox using MCSA and DWT.

References

[1] R.B. Randal, J. Hee, Cepstrum Analysis, Bruel and Kjaer Technical Review 3 (1981).
[2] N. Bayder, A. Ball, A comparative study of acoustic and vibration signals in detection of gear failures using Weigner–Ville distribution, Mechanical Systems and Signal Processing 15 (6) (2001) 1091–1107.
[3] C.J. Stander, P.S. Hayns, W. Schoombe, Using vibration monitoring for local fault detection on gears operating under fluctuating load conditions, Mechanical Systems and Signal Processing 16 (6) (2002) 1006–1024.
[4] F.A. Andrede, I.I. Esat, M.N.M. Badi, Gear condition monitoring by a new application of the Kolmogorov–Smirnov test, Proceeding of Institute of Mechanical Engineers—Part C 215 (2001) 653–661.
[5] C. Kar, A.R. Mohanty, Application of K S test in ball bearing fault diagnosis, Journal of Sound and Vibration 269 (1–2) (2004) 439–454.
[6] W. Wang, A.K. Wong, Some new signal processing approaches for gear fault diagnosis, Fifth International Symposium on Signal Processing and its Application, 1999, pp. 587–590.
[7] R.B. Randal, State of the art in monitoring rotor machinery, Proceeding of ISMA, vol-IV, 2002, pp. 1457–1478.
[8] W.J. Wang, P.D. McFadden, Application of wavelets to gearbox vibration signals for fault detection, Journal of Sound and Vibration 192 (5) (1996) 927–939.
[9] A. Yosida, Y. Ohue, H. Ishikawa, Diagnosis of tooth surface failure by wavelet transform of dynamic characteristics, Tribology International 33 (2000) 273–279.
[10] C.K. Sung, H.M. Tai, C.W. Chen, Locating defects of a gear system by the technique of wavelet transfer, Mechanism and Machine Theory 35 (2000) 1169–1182.
[11] N. Bayder, A. Ball, Detection of gear failures via vibration and acoustics signals using wavelet transform, Mechanical Systems and Signal Processing 17 (4) (2003) 787–804.
[12] Z.K. Peng, F.L. Chu, Application of the wavelet transform in machine condition monitoring and fault diagnostics: a review with bibliography, Mechanical Systems and Signal Processing 18 (2) (2004) 199–221.
[13] H.A. Gaborson, The use of wavelets for analyzing transient Machinery Vibration, Sound and Vibration (2002).
[14] M. Vetterli, C. Herley, Wavelets and filter banks: theory and design, IEEE Transaction on Signal Processing 49 (2) (1992) 2207–2232.
[15] J.R. Shadley, B.L. Wilson, M.S. Dorney, Unstable self-excitation of torsional vibration in AC induction motor driven rotational systems, Journal of Vibration and Acoustics, Transaction of ASME 114 (1992) 226–231.
[16] L. Ran, R. Yacamini, K.S. Smith, Torsional vibrations in electrical induction motor drives during start-up, Journal of Vibration and Acoustics, Transaction of ASME 118 (1996) 242–251.
[17] L. Eren, M.J. Devany, Motor bearing damage detection via wavelet analysis of the starting current transient, IEEE Instrumentation and Measurement Technology Conference, 2001, pp. 1797–1800.
[18] R.R. Schoen, T.G. Habetler, Effects of time-varying loads on rotor fault detection in induction machines, IEEE Transaction on Industry Applications 31 (4) (1995) 900–906.
[19] R.R. Schoen, B. Lin, T.G. Habetler, J.H. Schlag, S. Farag, An unsupervised, online system for induction motor fault detection using stator current monitoring, IEEE Transactions on Industry Application 31 (6) (1995) 1280–1286.
[20] C.M. Riley, B. Lin, T.G. Habetler, R.R. Schoen, A method for sensorless online vibration monitoring of induction machines, IEEE Transactions on Industry Application 34 (6) (1998) 1240–1245.
[21] R. Yacamini, K.S. Smith, L. Ran, Monitoring torsional vibrations of electro-mechanical systems using stator currents, Journal of Vibration and Acoustics, Transaction of ASME 120 (1998) 72–79.
[22] R.R. Schoen, T.G. Habetler, F. Kamran, R.G. Bartheld, Motor bearing damage detection using stator current monitoring, IEEE Transaction on Industry Applications 31 (6) (1995) 1274–1279.
[23] J.M. Aller, T.G. Habetler, R.G. Harley, R.M. Tallam, S.B. Lee, Sensorless speed measurement of AC machines using analytic wavelet transform, IEEE Transaction on Industry Applications 38 (5) (2002) 1344–1350.

[24] S.G. Mallat, A theory of multiresolution signal decomposition: the wavelet representation, IEEE Transaction on Pattern Analysis and Machine Intelligence 11 (7) (1989) 674–693.
[25] G. Strang, T. Nguyen, Wavelet and Filter Banks, Wellesley-Cambridge Press, 1996.
[26] F. Mayeux, E. Rigaud, J. Perret-Liaudet, Dispersion of critical rotational speeds of gearbox: effect of bearing stiffness, Proceedings of ISMA, vol. IV, 2002, pp. 1889–1896.
[27] S. Theodossiades, S. Natsiavas, Periodic and chaotic dynamics of motor-driven gear-pair systems with backlash, Chaos, Solitons and Fractals 12 (2001) 2427–2440.